OVERPRINTING DEFORMATIONS IN MANTLE ROCKS, DUN MOUNTAIN, NEW ZEALAND

A Thesis

by

SARA MICHELLE DONNELLY

Submitted to the Office of Graduate and Professional Studies of
Texas A&M University
in partial fulfillment of the requirements for the degree of

MASTER OF SCIENCE

Chair of Committee,	Julie Newman
Committee Members,	Will Lamb
	Deborah Thomas
Head of Department,	John R. Giardino

May 2014

Major Subject: Geology

ABSTRACT

Dun Mountain is the northern-most ultramafic massif of the Dun Mountain Ophiolite Belt, South Island, New Zealand, and is the type-locale of dunite. The dunites that are preserved at this location provide an opportunity for studying olivine rheology over a range of naturally-occurring mantle temperatures, pressures, stresses, and strain rates. Field observations include mesoscale dunite and harzburgite compositional bands ranging from 1 cm to 1 m in scale and oriented at 038°, 40° SE. Spinel lineations are oriented at 004°, 40° and lie approximately in the plane of the compositional bands. Thin sections oriented perpendicular to the compositional bands and parallel to the spinel lineations show olivine bi- and tri- modal grain size distributions and olivine exhibits undulose extinction, subgrains, and a shape-preferred orientation. Olivine lattice preferred orientation indicates "pencil glide" or that the (010)[100] and (001)[100] slip systems were active. In harzburgite, straight and aligned phase boundaries occur between olivine and orthopyroxene grains and microscale olivine and orthopyroxene compositional bands. Olivine microstructures suggest deformation was accommodated by dislocation creep and, in harzburgite, by dislocation creep and phase boundary sliding. Olivine grain size and grain size distributions in dunite and harzburgite are similar, suggesting that phase boundary sliding in harzburgite occurred due to the presence of orthopyroxene, and not due to a finer olivine grain size..

Grain size analyses of olivine indicate grain size distributions containing three populations of grain size with average chord lengths of 5, 1.8, and 0.4 mm. A stress piezometer empirically fit to the experimentally derived relationship between stress and

dynamically recrystallized grain size suggests stresses of 2, 5 and 15 MPa, respectively, for these chord lengths. Two-pyroxene thermometry suggests that the intermediate grain size population deformed at 1100 °C, while the finer grain size population deformed at lower temperatures, perhaps as high as 950 °C. Mineral equilibria in plagioclase-bearing spinel peridotite yields pressures of 550 to 600 MPa at these temperatures. Deformation mechanism maps based on olivine flow laws at 950 and 1100 °C both suggest strain rates of 10^{-13} s^{-1}. Olivine flow law and stress piezometry indicate deformations at a constant strain rate while stresses increased in response to decreasing temperature conditions.

ACKNOWLEDGEMENTS

I would like to thank my committee chair, Dr. Newman, and my committee members, Dr. Lamb, Dr. Thomas for their guidance and support throughout the course of this research. I also want to thank Dr. Basil Tikoff, Eric Stewart, Dr. Seth Kruckenberg, and Zachary Michels for all the assistance in the field. This research was support by the National Science Foundation grant EAR-1050044 to Julie Newman, Will Lamb, Basil Tikoff, and Seth Kruckenberg.

I would also like to thank Caleb Holyoke, Ray Guillemette, Rachel Wells, and Tom Stephens, for their support and assistance.

Finally, thanks to my parents, my sister, and my friends for all the support and encouragement.

NOMENCLATURE

disGBS	Dislocation-accommodated grain boundary sliding
DMOB	Dun Mountain Ophiolite Belt
EBSD	Electron backscatter diffraction
HREE	Heavy rare earth element
ICP-MS	Inductively coupled plasma-mass spectrometry
LPO	Lattice preferred orientation
LREE	Light rare earth element
P	Pressure
PBS	Phase boundary sliding
REE	Rare earth element
SEM	Scanning electron microscopy
SPO	Shape preferred orientation
T	Temperature

TABLE OF CONTENTS

Page

LIST OF FIGURES

Page

LIST OF TABLES

Page

1. INTRODUCTION

The strength and deformation of the upper mantle play an important role in determining the behavior of tectonic plates. The relationship between stress, strain rate, and temperature during mantle deformation is still subject for debate. Workers argue that mantle flow is either dominated by constant stress, strain rate or a combination of both, which are imposed by the movement of tectonic plates (DeMets and Dixon, 1999; Platt and Behr, 2011). Deformations at constant strain rate or constant stress have implications for localization as well as which deformation mechanisms are active (Dunlap et al., 1997; Platt and Behr, 2011; Hansen et al., 2012a). Understanding these relationships as well as the nature of deformation in poly- and mono- mineralic rocks give insight to natural deformations in the mantle.

Understanding of mantle deformation comes from coupling studies of deformation of olivine and pyroxene in the laboratory, modelling of the lithosphere, and rheological field studies (Walcott, 1965; Carter and Ave'lallemant, 1970; Brace and Kohlstedt, 1980; Regenauer-Lieb et al., 2001). Field studies rely primarily on the ultramafic sections of ophiolite sequences for evidence of deformation at naturallyoccurring temperatures, pressures, stresses, and strain rates (e.g. Newman et al., 1999; Webber et al., 2008; Toy et al., 2010). The ultramafic massifs of the Dun Mountain Ophiolite Belt (DMOB), New Zealand are well exposed and minimally serpentinized, offering an opportunity to investigate the relationships between stresses and strain rates during upper mantle deformation.

Christensen (1984) describes Dun Mountain, the type-locale of dunite, as having dunite/harzburgite banding, olivine lattice preferred orientation (LPO), and a spinel lineation. This current work extends this characterization by characterizing the rheology of the Dun Mountain rocks while they experienced uplift at upper mantle conditions. I address the following questions: *i.) What deformation mechanisms were responsible for accommodating deformation of the Dun Mountain rocks? ii.)What were the stresses and strain rates during deformation, and under what pressure and temperature conditions did these rocks deform? iii.) How does Dun Mountain relate to the other ultramafic massifs of the Dun Mountain Ophiolite Belt?*

Olivine microstructures in dunite and harzburgite suggest deformation occurred by dynamic recrystallization accommodated dislocation creep and, in harzburgite, by phase boundary sliding. Similar olivine grain size distributions in harzburgite and dunite suggest that phase boundary sliding in harzburgite, which accompanied dislocation creep in olivine, was due to the presence of ~25% orthopyroxene, and not due to grain size reduction of olivine. Olivine flow laws used to create deformation mechanism maps suggest that deformations in the lithospheric upper mantle occurred at progressively decreasing pressure/temperature conditions, increasing differential stress, and at a constant strain rate of 10^{-13} s^{-1}. These results are consistent with those of workers who have proposed stress varies as a function of temperature and strain rate during deformation of the crustal lithosphere (Dunlap et al., 1997; Behr and Platt, 2011).

2. GEOLOGIC SETTING

The mafic and ultramafic rocks of the DMOB, South Island, New Zealand, are divided into the northern Nelson segment, and the southern Otago segment, separated by the Alpine fault. The Otago ultramafics are found at Red Mountain and the Nelson ultramafics occur at both Dun Mountain and the Red Hills (Figure 1). Walcott (1965), Christensen (1984); Webber et al. (2008), and Stewart et al. (in prep.), describe the composition and structures of the Red Hills and Dun Mountain massifs.

Walcott (1965) separated the Red Hills complex into two domains: a non-foliated domain of massive harzburgite, and a domain dominated by compositional banding of harzburgite, dunite and gabbro, cross-cut by pyroxenite dikes. Walcott proposed a tectonic origin for the foliations, lineations, and olivine shape and lattice preferred orientation (S- and L-PO) he described at the Red Hills. More recently, Webber et al. (2008) mapped a 2 km^2 portion of the Red Hills massif, near Porter's Knob, and identified four structural domains defined by different orientations of juxtaposed harzburgite/dunite compositional bands, a ~50 m thick shear zone, harzburgite/lherzolite compositional bands, and lherzolite with olivine/pyroxene compositional bands. These domains revealed a history of overprinting and suggested spatially heterogeneous deformations on the decimeter to kilometer scale, similar to the scale of deformation and localization often observed in crustal rocks. Recent mapping of the entire Red Hills massif (Stewart et al., in prep.) is consistent with these observations, and also outlines the evolution of the observed overprinting deformations.

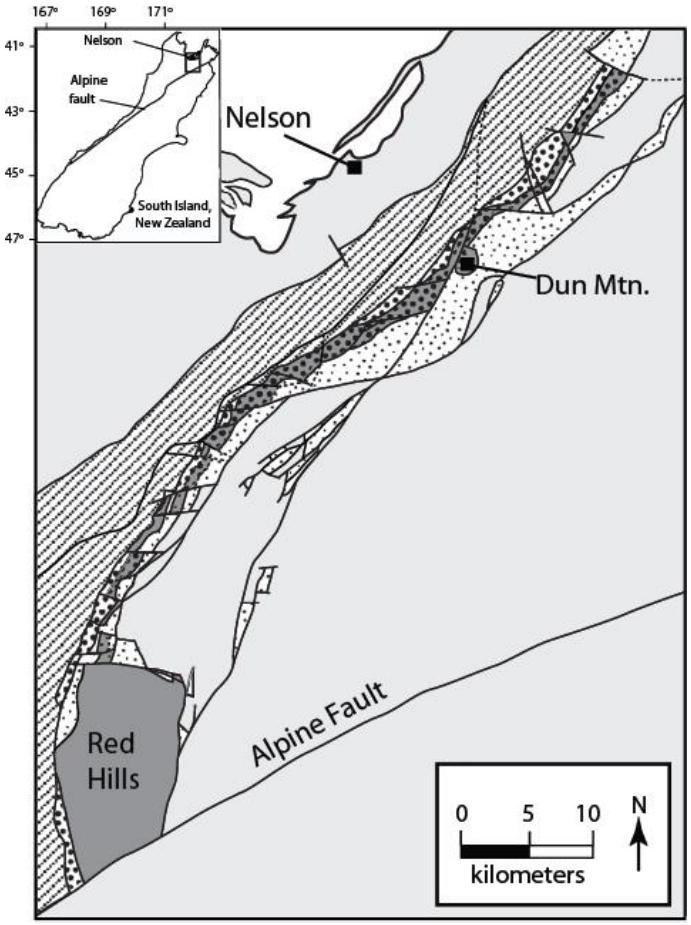

Figure 1: Map of the Nelson segment of the Dun Mountain Ophiolite Belt. Segment includes the Red Hills and Dun Mountain ultramafic massifs. Modified from Webber et al. (2008).

The overprinting fabrics combined with the geochemistry of the defined domains at Red Hills reveal a tectonics evolution beginning with deformation at a mid-ocean ridge spreading center to later deformation in a supra-subduction environment (Stewart et al., in prep.)

The Dun Mountain massif (Figure 2), the northernmost ultramafic section of the DMOB and the type-locale for dunite, has been characterized most recently by Christensen (1984). He proposed an upper mantle origin for Dun Mountain and described a meter-scale, northeast-striking foliation defined by harzburgite and dunite compositional bands, a lineation defined by elongate olivines and spinels, and porphyroclastic textures. Christensen also measured a strong olivine a-axis LPO subparallel to the harzburgite/dunite compositional bands and a weak LPO in orthopyroxene. Based on these observations, Christensen (1984) concluded that Dun Mountain had experienced high temperature flow with a dextral shear sense.

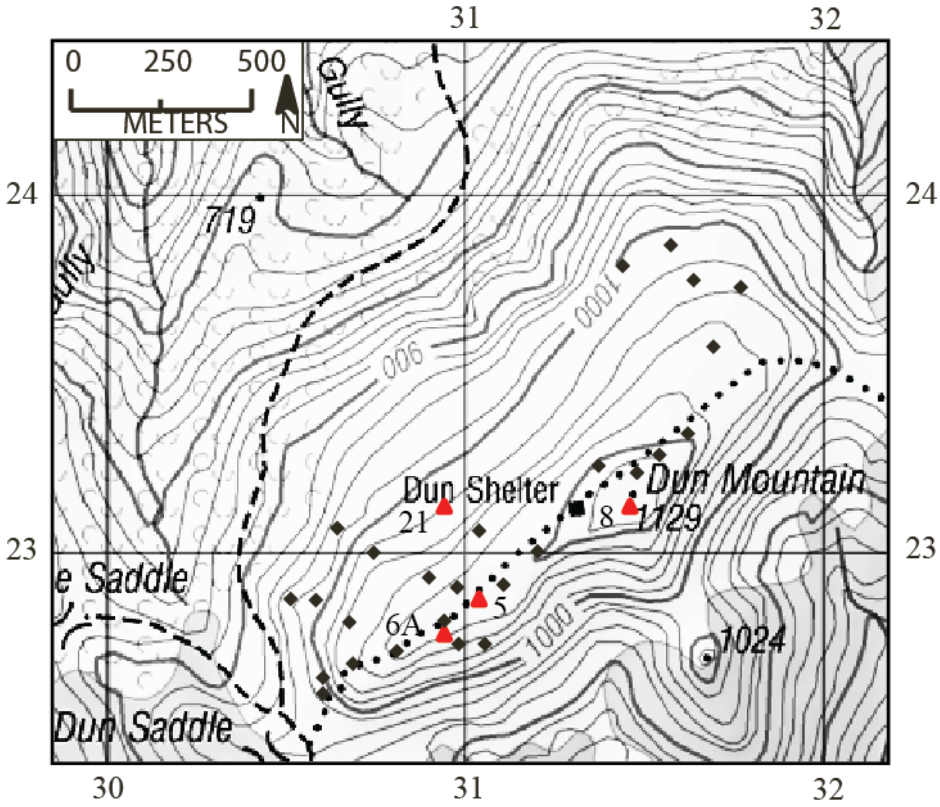

Figure 2: Local map of Dun Mountain. Field data and samples were collected at sites denoted by diamonds and triangles. Red triangles indicate locations of samples chosen for further study.

3. METHODS

Field measurements (e.g., foliations, lineations) were made at 29 locations across the massif and a total of 32 samples were collected from these locations. Microstructural analyses from these samples, including grain size and shape analyses, were carried out on thin sections cut perpendicular to the foliation (defined by compositional banding) and parallel to lineation (defined by elongated spinels) measured in the field. I used two methods to characterize grain size: image processing software (*Image SXM*, Barrett (2008)) and the mean lineal intercept method. Analyses using both methods were carried out on diagrams produced by tracing grain boundaries on optical scans of entire thin sections.

Image analysis allows determination of shape-preferred orientation and the orientation of long axes in addition to estimating grain size. Image SXM assumes an ellipse for traced grains and determines the lengths of the long and short axes, and orientation of the long axes relative to a chosen reference frame.

The mean lineal intercept method measures chord lengths of intersected grains in linear transects across a thin section. Three transects in each orientation (parallel, perpendicular, and at 45˚ to the olivine shape preferred orientation (SPO) determined from image analysis) are made to gather approximately 200 chord measurements per sample. These measurements are resolved into statistical distributions using Spektor's Chord analysis as outlined by Underwood (1970). Spektor's Chord analysis derives a grain size distribution by determining the number of particles per unit volume from these chord lengths using the equation:

$$(N_V)_j = \frac{4}{\pi\Delta^2}\left[\frac{(n_L)_j}{2j-1} - \frac{(n_L)_{j+1}}{2j+1}\right] \qquad (1)$$

where $(N_V)_j$ and $(n_L)_j$ are the number of particles per unit volume and the number of chords per unit length of the transect, respectively, for the indicated j bin size, and Δ is the bin size (Underwood, 1970). Olivine LPO data were obtained on a scanning electron microscope (SEM; FEI Quanta 600) housed at Texas A&M University using electron-backscattered diffraction (EBSD; Channel 5, Oxford Instruments). EBSD mapping of harzburgite was conducted using EBSD at the SEM laboratory in Boston College (Tescan Vega 3 LMU).

Modal mineralogy for each sample was determined by calculating the percent of the total line length of each mineral (olivine, orthopyroxene, clinopyroxene, spinel, and plagioclase) from the lineal analysis transects. Mineral compositions were determined using a Cameca SX50 electron microprobe at Texas A&M University. Olivine, spinel, orthopyroxene, and clinopyroxene were analyzed using a 15 kV accelerating voltage, a 20 nA beam current, and a 1 micron beam diameter. In order to avoid electron beam-induced sodium diffusion, feldspars were analyzed with a 10 nA beam current. The weight percent oxides were normalized to the number of cations in each mineral (e.g. pyroxenes to four, olivine and spinel to three, and plagioclase to five). Geothermobarometric estimates were carried out within the context of the microstructural observations. For example, large and small grains that might represent porphyroclasts and recrystallized grains, respectively, and that are in close proximity are grouped accordingly for purposes of geothermobarometric estimates. Sample 12DM-5 contains clinopyroxene exsolution lamella in host orthopyroxene grains that were

reintegrated by analyzing the host and lamellae, then calculating the original composition using the percentage by area of each (Bohlen and Essene, 1977). Inductively coupled plasma-mass spectrometry (ICP-MS) analyses of trace and rare earth elements were carried out at the Washington State University GeoAnalytical Laboratory.

4. RESULTS

4.1 Field observations

The Dun Mountain massif contains massive dunites, banded dunites and harzburgites, chromite seams, and pyroxenite dikes (Figure 3). Dunite and harzburgite compositional bands range from a centimeter to a meter in thickness and have an average orientation of 038°, 40° SE. Spinel lineations lie approximately parallel to the strike of the compositional banding, with an average orientation of 04°, 040°. The mesoscale compositional banding and lineation orientations are similar to those reported by Christensen (1984) with fabrics subparallel to the length of Dun Mountain, trending northeast/southwest. The chromite seams range in thickness from millimeter to centimeter scale and have an average orientation of 032°, 35° SE. They are most abundant in the southern parts of the massif. Pyroxenite dikes are thin (millimeter to centimeter scale) and cross-cut the dunite in a nonsystematic range of orientations (Figure 4).

Massive dunite occurs most extensively in the northern portions of the massif. The orthopyroxene content of the host rocks varies from <1 to ~25% volume across the massif, but the harzburgite banding grades from the centimeter to the meter scale moving from the southern to the central portions of Dun Mountain. Clinopyroxene is less prevalent than orthopyroxene (there are no lherzolites or wherlites at Dun Mountain) but accounts for ~3% of the host rock volume, present primarily in a small, irregularly-shaped pocket of clinopyroxene and plagioclase-bearing dunites on the southeastern side

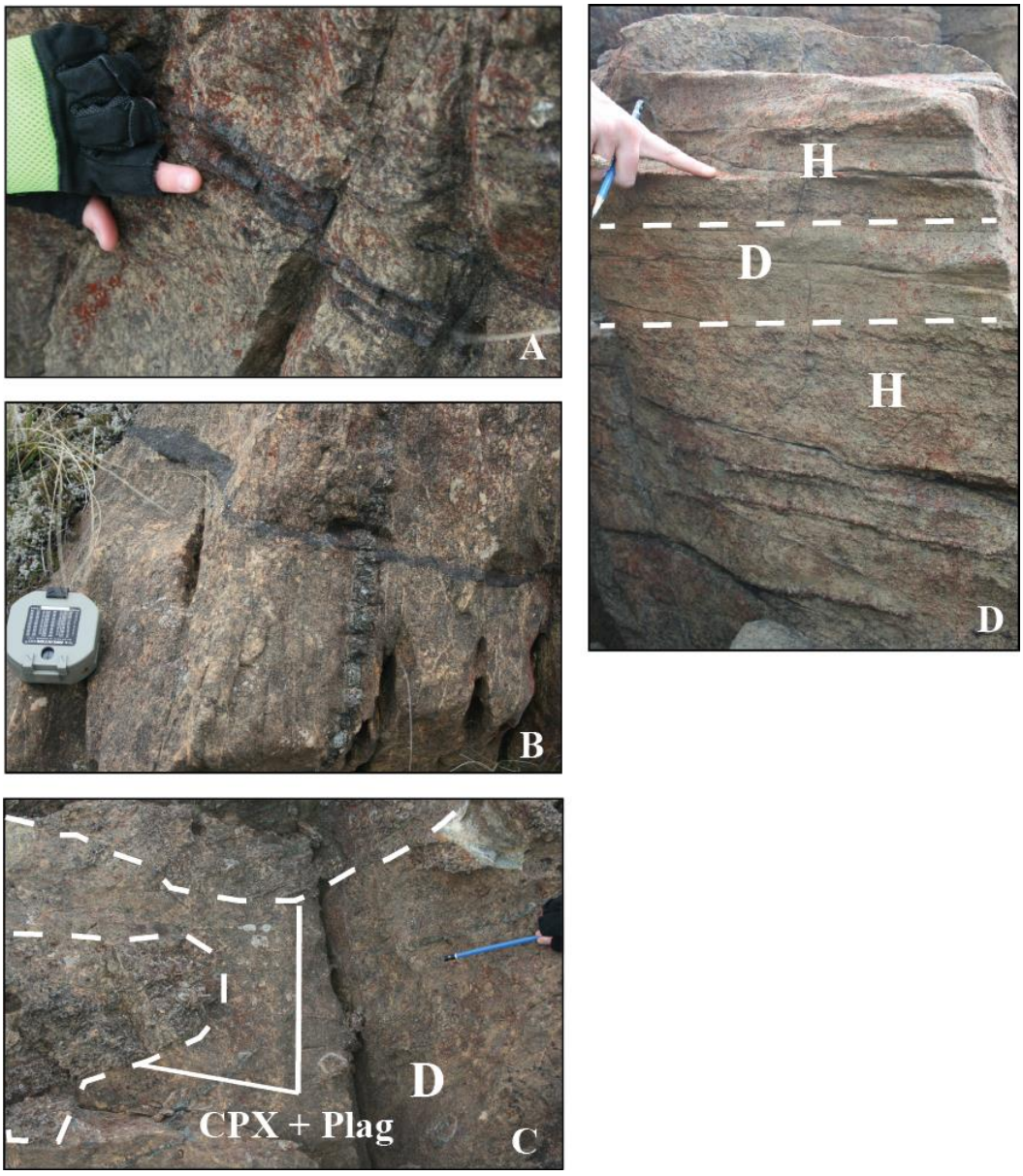

Figure 3: Dun Mountain structures: (A) chromite seams, (B) centimeter-scale dunite (D) and harzburgite (H) compositional bands, (C) pyroxenite dike and chromite seam, (D) plagioclase-bearing dunite pod.

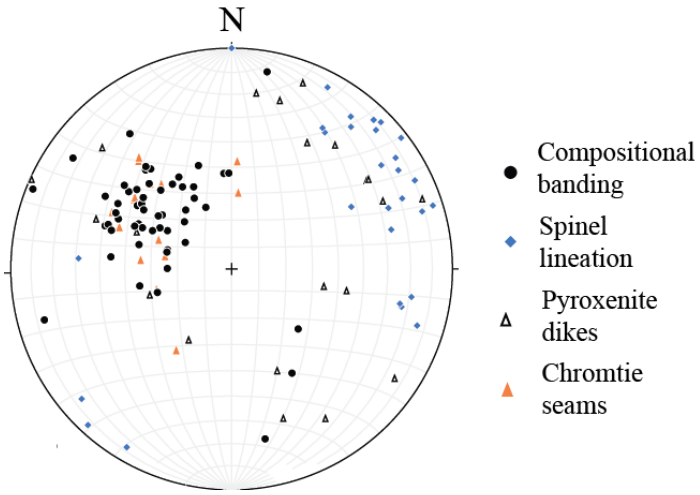

Figure 4: Equal area, lower hemisphere projection of the orientation of chromite seams, pyroxenite dikes, and harzburgite/dunite compositional bands, n=114.

of the massif. This pod is discordant with the measured foliations (Figure 3d). Sampling from this area yields the five phase assemblage (olivine, spinel, orthopyroxene, clinopyroxene, and plagioclase) required to estimate pressures from mineral equilibria (see section 4.3.2; Geothermobarometry). Pyroxenite dikes are distributed throughout the massif and contain both ortho- and clinopyroxene but are generally ~90% or more clinopyroxene, with smaller amounts, <10%, orthopyroxene. These dikes are within the center of dunite bands, or cross-cut dunite/harzburgite bands, and have linear, folded, and en echelon geometries.

4.2 Microstructures

Of the 32 collected samples, 11 were chosen for characterization of deformation microstructures based on spatial distribution across the massif, representative compositions, and lack of serpentinization (Figure 2). The northern portions of the massif have experienced slumping and a higher degree of serpentinization, so samples from this portion were not used for microstructural study. The eleven samples were then narrowed down further to four (12DM-5, 12DM-6A, 12DM-8, and 12DM-21) representative samples that display a range of microstructures (e.g., grain size) and compositions recorded by these rocks (Figure 5; Table 1). All thin sections are oriented perpendicular to the harzburgite/dunite compositional bands, and parallel to spinel lineations measured in the field.

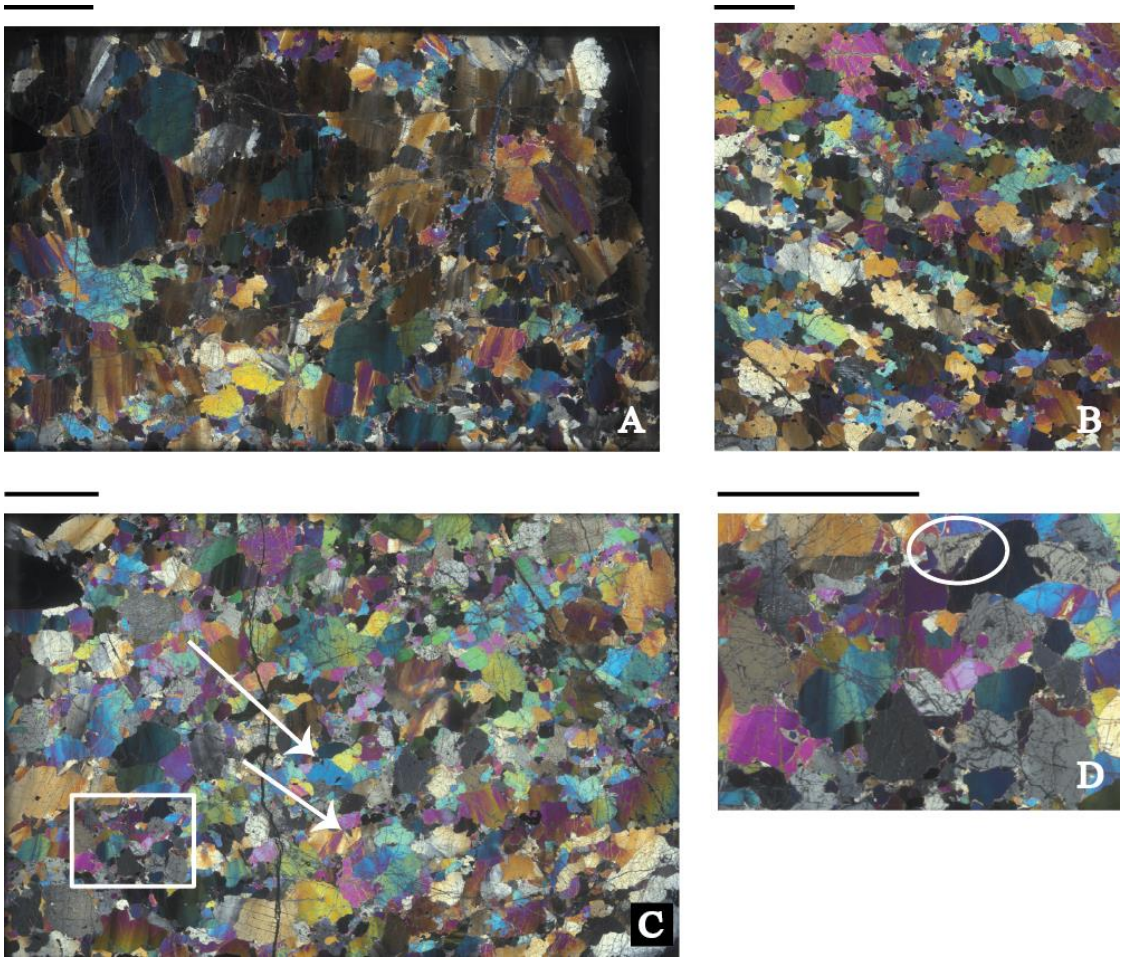

Figure 5: Dunite and harzburgite microstructures. All scale bars are 4 mm. (A) Dunite (12DM-8) with trimodal olivine grain size distribution. Olivine grains in this sample have chord lengths up to 8 mm. (B) Dunite (12DM-6A) with bimodal olivine grain size distribution. Olivine grain size distribution is the same as in harzburgite (C). (C) Harzburgite with bimodal olivine grain size distribution. Microscale compositional bands and aligned grain boundaries (arrows) occur between olivine and orthopyroxene. (D) Inset shown in (C) displaying orthopyroxene with acute grain boundaries.

Table 1

Modal Mineralogy

Sample No.	Olivine	Orthopyroxene	Clinopyroxene	Spinel	Plagioclase
12DM-5*	70%	25%	2%	1%	0%
12DM-6A	93%	<1%	3%	1%	2%
12DM-8	97%	1%	1%	1%	0%
12DM-21*	96%	<1%	<1%	1%	0%

*Remainders are fractured or serpentinized areas.

The samples exhibit a porphyroclastic microstructure and application of the Spektor chord analysis to the four samples analyzed yields bi- and tri- modal grain size distributions of olivine (coarse >4.2 mm, intermediate 0.9-4.2 mm, and fine <0.9 mm) (Figure 6). The means of these populations are 5.0, 1.8, and 0.4 mm, respectively. Olivine grains in all 11 samples display undulose extinction in intermediate and coarse grains, and subgrains. Grain shape analyses using Image SXM software (Barrett, 2008) show that olivine grains are elongate (~2.1 axial ratio) with long axes subparallel to the harzburgite/dunite compositional banding measured in the field (Figure 6). When pyroxene is present (in dunite and harzburgite), some ortho- and clino-pyroxenes have acute grain boundaries and surround or partially surround other grains (Figure 5d).

4.2.1 Dunite

Olivine grain size distributions in dunite are either bi- or tri- modal (>4.2 mm, 0.9-4.2 mm, and <0.9 mm), with the coarsest grain size population absent in bimodal samples. Olivine a-axes show a LPO with a point maximum subparallel to the foliation defined by the olivine SPO and b- and c- axes a-axes are weaker girdles (Figure 7). Separate stereoplots of the different olivine grain size populations indicate that the LPO is not grain size dependent.

4.2.2 Harzburgite

In harzburgite, there are microscale (~2 mm thick) bands defined by alternating dominantly olivine and dominantly orthopyroxene compositional bands and the grain

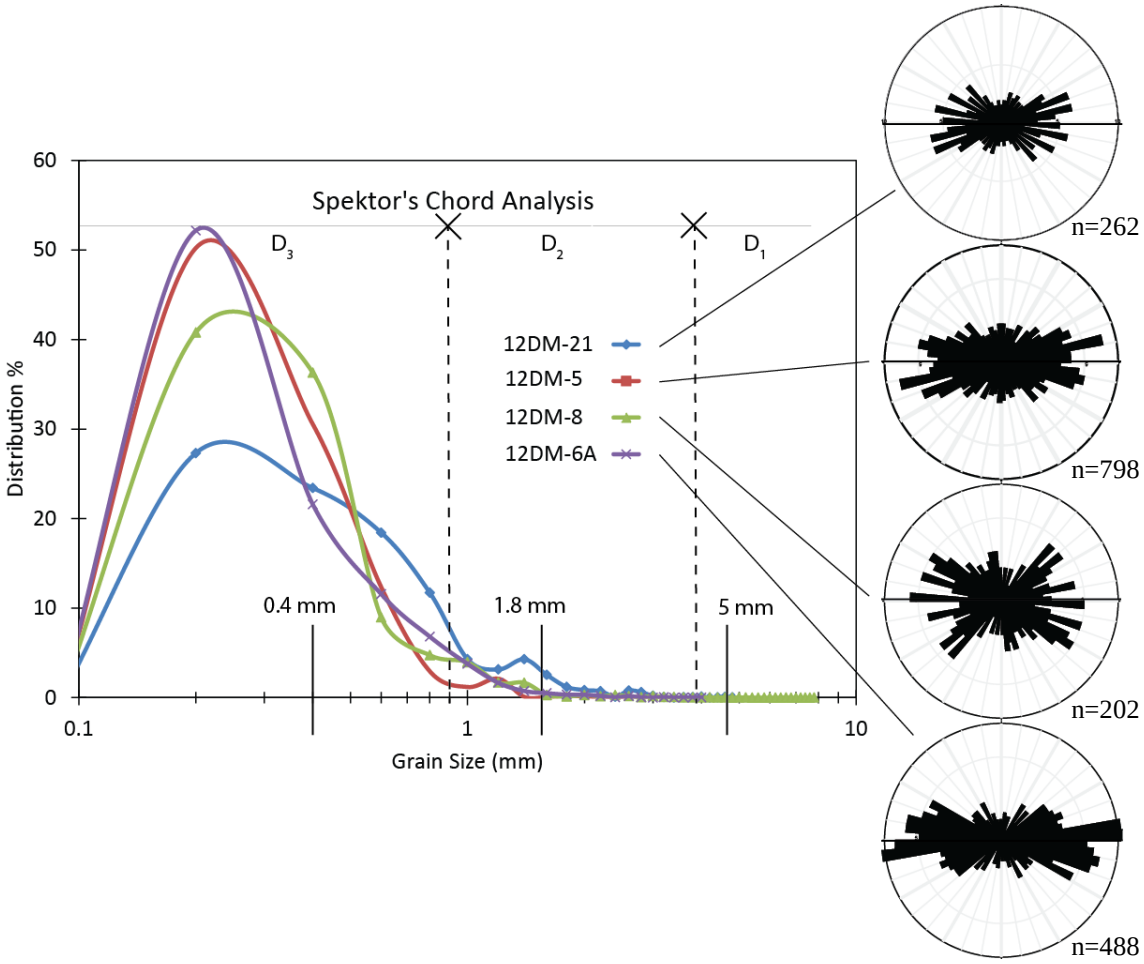

Figure 6: Olivine grain size distributions resolved by Spektor's chord analysis. 12DM-5 is harzburgite, and the other three samples (6A, 8, and 21) are dunite. Grain size populations are denoted by D_n and the calculated means for each population are 5, 1.8, and 0.4 mm (marked on the x-axis). Samples 12DM-8 and 12DM-21 are dunites and the only two samples with the coarsest olivine grain size population. Rose diagrams (perimeter=8%) show olivine SPO relative to the average orientation of olivine SPO in each sample (horizontal); the average axial ratio is 2.1.

boundaries are linear between the two phases (Figure 5). The olivine grain size distribution in harzburgite is bimodal and only contains fine (<0.9 mm) and intermediate (0.9-4.2 mm) olivine grain size populations.

Olivine in harzburgite has a LPO similar to olivine in dunite with a strong a-axis point maximum, and slightly weaker girdling of the b- and c-axes (Figure **7**). Orthopyroxene in this sample also has a very weak LPO (Figure **7**).

Harzburgite and bimodal dunite have the same grain size distributions (i.e. same populations and same mean grain size of each population), but the harzburgite has straight and aligned phase boundaries between olivine and orthopyroxene grains and microscale olivine and orthopyroxene bands. The bimodal dunite has slightly irregular grain boundaries, and even though there is a strong SPO, the alignment of linear grain boundaries observed in the harzburgite is absent.

4.3 Petrology

4.3.1 Mineral chemistry

Compositions of analyzed olivine, spinel, orthopyroxene, clinopyroxene, and plagioclase are summarized in Table 2. All grains were analyzed along transects using approximately 100-150 μm spacing between analytical points. Olivine grains of all sizes are homogeneous with no apparent zoning (measured from transects). Zoning in pyroxenes is not apparent, however, BSE imaging revealed clinopyroxene lamellae in several coarse orthopyroxenes in harzburgite. Several intermediate

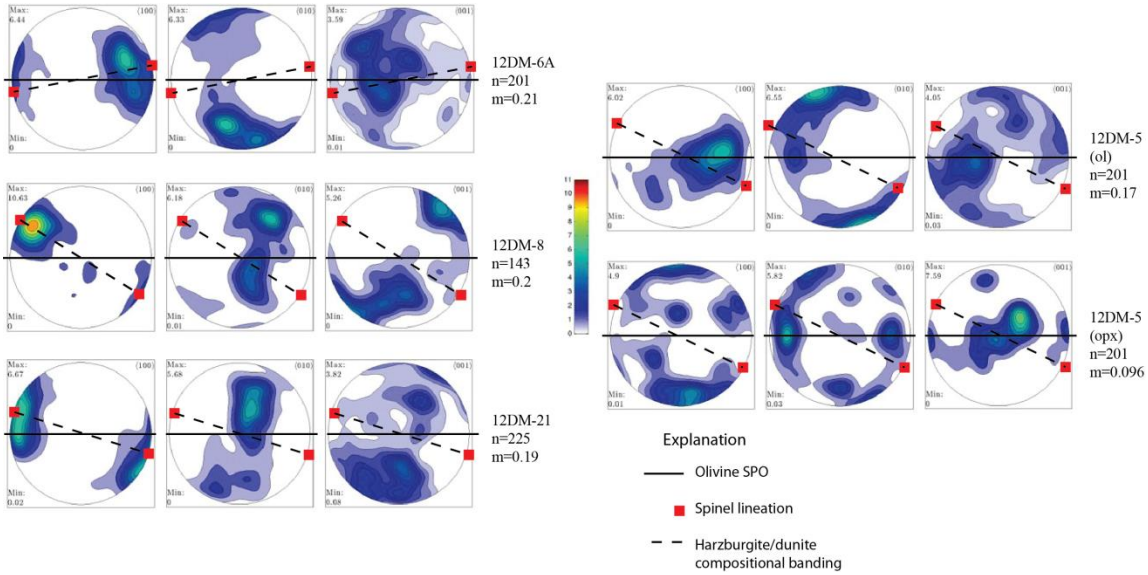

Figure 7: EBSD data showing olivine LPO in dunite (left) and olivine and orthopyroxene in harzburgite (right). Data are plotted relative to the elongation of olivine (SPO) for each sample, which is the horizontal. Olivine LPO is weaker in harzburgite than in dunite and orthopyroxene LPO in harzburgite is very weak.

Table 2

Mineral Compositions

Sample	12DM-6A					12DM-21		12DM-5				12DM-8			
Phase	ol	opx	cpx	sp	plag	ol	sp	ol	*opx	cpx	sp	ol	opx	cpx	sp
Wt% oxides averaged															
SiO_2	40.86	57.89	52.73	0.01	44.14	40.81	0.02	41.20	55.91	53.08	BDL	41.00	57.00	54.12	BDL
TiO_2	NA	0.01	0.08	0.05	NA	NA	0.35	NA	0.02	0.04	0.09	NA	0.02	0.04	0.13
Al_2O_3	BDL	0.62	3.10	36.95	36.95	BDL	21.01	BDL	1.93	2.14	21.57	BDL	1.23	1.16	17.39
Cr_2O_3	NA	0.07	0.88	29.61	NA	NA	37.64	NA	0.62	0.96	46.02	NA	0.44	0.53	49.11
V_2O_3	NA	NA	NA	0.12	NA	NA	0.24	NA	NA	NA	0.28	NA	NA	NA	0.26
FeO	10.87	6.99	2.22	18.26	0.07	9.99	29.16	9.67	5.94	2.33	20.83	9.52	6.23	1.78	21.65
MnO	0.16	0.19	0.06	0.43	BDL	0.16	0.59	0.14	0.15	0.06	0.62	0.14	0.14	0.05	0.68
NiO	0.33	0.08	0.03	0.14	NA	0.27	0.14	0.38	0.09	0.04	0.08	0.37	0.07	0.03	0.09
MgO	48.86	34.54	17.04	14.70	BDL	49.33	10.23	50.11	33.47	17.59	11.81	50.07	34.65	18.01	10.73
CaO	0.02	0.32	24.18	0.02	19.84	0.06	BDL	0.02	1.22	23.92	BDL	0.03	0.76	24.25	BDL
Na_2O	0.01	0.00	0.20	NA	0.43	0.01	NA	0.01	0.00	0.19	NA	0.01	0.02	0.13	NA
Total	101.12	100.72	100.52	100.48	101.45	100.64	99.58	101.53	99.37	100.37	101.14	101.16	100.57	100.09	100.23

*These are reintegrated

BDL=below detection limits

Normalized Values

Sample	12DM-6A					12DM-21		12DM-5				12DM-8			
Phase	ol	opx	cpx	sp	plag	ol	sp	ol	*opx	cpx	sp	ol	opx	cpx	sp
Wt% oxides averaged															
Si	0.9946	1.9886	1.8992	0.0003	2.0140	0.9910	0.0005	0.9930	1.9434	1.9187	0.0001	0.9912	1.9534	1.9581	0.0001
AlIII		0.0114	0.1008	1.2640	1.9870		0.7574		0.0566	0.0813	0.7821		0.0466	0.0419	0.6528
AlIV	0.0001	0.0096	0.0357					0.0001	0.0225	0.0099		0.0002	0.0030	0.0075	
Ti		0.0014		0.0010			0.0084		0.0005	0.0012	0.0021		0.0006	0.0010	0.0032
Cr		0.0014	0.0260	0.6742			0.9870		0.0171	0.0275	1.1197		0.0119	0.0151	1.2368
V				0.0000							0.0000				0.0000
FeIII			0.0520	0.0159	0.0030		0.2255		0.0159	0.0547	0.0487		0.0317	0.0265	0.0566
FeII	0.2212	0.1969	0.0224	0.4210		0.2148	0.5634	0.1950	0.1567	0.0158	0.4875	0.1925	0.1469	0.0273	0.5201
Mn	0.0033	0.0057	0.0019	0.0053		0.0035	0.0085	0.0028	0.0044	0.0019	0.0161	0.0030	0.0042	0.0015	0.0185
Ni	0.0064	0.0021	0.0009	0.0029		0.0054	0.0034	0.0074	0.0026	0.0013	0.0019	0.0073	0.0020	0.0008	0.0022
Mg	1.7731	1.7713	0.9126	0.6150		1.7825	0.4567	1.8009	1.7346	0.9481	0.5416	1.8044	1.7704	0.9711	0.5096
Ca	0.0006	0.0122	0.9294	0.0004	0.9700	0.0021		0.0004	0.0457	0.9262	0.0001	0.0009	0.0280	0.9399	0.0001
Na	0.0006	0.0003	0.0168		0.0380	0.0003		0.0003	0.0000	0.0131	0.0000	0.0004	0.0012	0.0092	
Sum	3.0000	4.0000	4.0000	3.0000	5.0000	3.0000	3.0000	3.0000	4.0000	4.0000	3.0000	3.0000	4.0000	4.0000	3.0000

clinopyroxenes in dunite contain blebs of orthopyroxene (2-3 μm) at grain boundaries that may be the result of exsolution as well.

Spinels are chrome-rich and do not show major trends between fine and coarse grains, but several fine grains exhibit lower chromium in the rims. In these cases, the core compositions are used for geothermometry. Plagioclase grains (found in sample 12DM-6A) are ~97% anorthite and compositions do not vary significantly between grains.

ICP-MS analyses of trace elements are normalized to the primitive mantle as outlined by Sun and McDonough (1989). These normalized values show enrichment in both heavy and light rare earth elements (H- and L- REEs), or a u-shaped pattern graph (Figure 8). The bulk rock chemistry, also normalized to the primitive mantle, shows a negative (or depleted) niobium trend in the trace element profile.

4.3.2 Geothermobarometry

Two-pyroxene geothermometry is relatively well-calibrated and has been widely applied to determine temperatures in spinel peridotites. However, a number of formulations to two-pyroxene geothermometry have been developed (Wells, 1977; Brey and Köhler, 1990; Taylor, 1998; Nimis and Grütter, 2009) and application of this geothermometer requires choosing the most appropriate formulation. *Nimis and Grütter (2009)* compared a number of these two-pyroxene formulations and argued that the thermometer developed by Taylor (1998) most accurately reproduced temperatures of laboratory experiments designed to equilibrate co-existing pyroxenes. We have applied

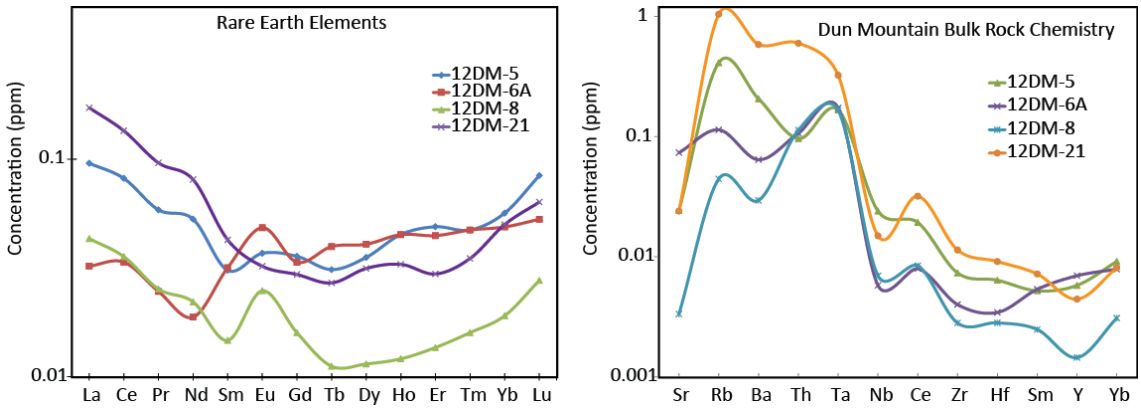

Figure 8: REE and trace element chemistry of samples measured in ICP-MS analyses. REE profile shows enrichment of both heavy and light REEs. Trace element profile shows depletion of niobium (Nb).

the Taylor (1998) two-pyroxene geothermometer in an effort to estimate temperatures of deformation from the compositions of co-existing pyroxenes.

According to Nimis and Grütter (2009), the temperatures determined using Taylor (1998) two-pyroxene thermometer are most sensitive to the composition of clinopyroxene (cpx), and are not strongly dependent on the composition of orthopyroxene (opx), even though both pyroxenes must be in equilibrium. However, the Brey and Köhler (1990) calcium-in-orthopyroxene thermometer is, as the name implies, sensitive to the composition of only the opx, even though, again, both cpx and opx must be in equilibrium. Nimis and Grütter (2009) modified the Brey and Köhler (1990) calcium-in-orthopyroxene thermometer so that temperature estimated with the thermometer agree with those calculated using Taylor (1998) two-pyroxene geothermometer to within ±30°C. Thus, if the opx and cpx are in equilibrium then temperatures estimated with these two thermometers should agree to within ±30˚C (Nimis and Grütter, 2009).

Analyzed pyroxenes are grouped based on proximity and microstructure (i.e. grain size) in an attempt to identify grains that deformed under similar deformation conditions. Care was taken not to estimate temperatures from grains that showed evidence of melt structures (e.g. acute grain boundaries). The results of the pyroxene geothermometry are summarized in Figure 9.

The highest temperatures were reintegrated using the compositions of exsolved orthopyroxenes that fall within the intermediate grain size population (0.9-4.2 mm). These orthopyroxenes have no texturally equivalent clinopyroxenes and, as a result,

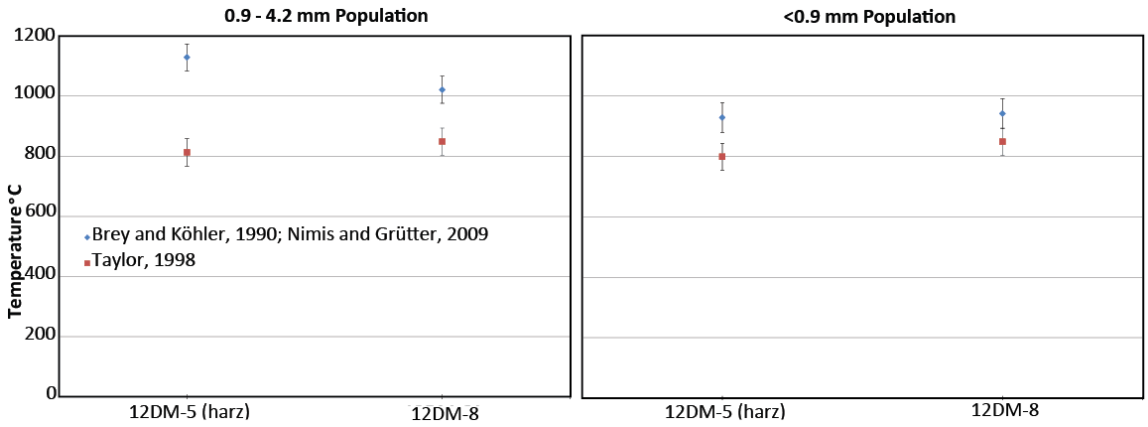

Figure 9: Comparison of pyroxene thermometers for intermediate (left) and fine (right) grain size populations. Taylor (1998) estimates are consistently lower than Brey and Köhler (1990) estimates by 150 °C or more.

temperatures for these orthopyroxenes are based solely on the Brey and Köhler (1990) Ca-in-opx geothermometer as modified by Nimis and Grütter (2009). Only two orthopyroxene grains, both from sample 12DM-5 have cpx exsolution that we were able to reintegrate, and these reintegrated opx grains yield temperatures of 1080 to 1130 °C.

Intermediate opx grains from sample 12DM-8, with no detectable exsolution, yield temperatures of 990 to 1015 °C using the modified Ca-in-opx geothermometer. This same geothermometer yields temperatures of 930 to 940 °C for smaller opx grains (<0.9 mm) from samples 12DM-5 and 12DM-8. Based on these data we suggest that larger (intermediate size) opx grains equilibrated at T≈1100 °C whereas the small opx grains record lower temperatures, with some temperatures as high as ≈950 °C.

All cpx grains belong to the fine grain size population (< 0.9 mm), and the Taylor (1998) two-pyroxene temperatures for all samples fall between 730 and 850˚C. As discussed previously, this thermometer is largely sensitive to the composition of the cpx, suggesting that this mineral equilibrated at these relatively low temperatures. One sample, 12DM-6A exhibits good agreement between temperatures based on Taylor's (1998) two-pyroxene geothermometer and the Ca-in-opx geothermometer of Brey and Kohler as modified by Nimis and Grütter (2009).

Equilibrium pressures from the two temperature regimes (1100 °C and 950 °C) were estimated from the equilibrium:

spinel + diopside + enstatite = anorthite +2forsterite (2)

in the plagioclase bearing sample (12DM-6A). End-member activities of plagioclase (anorthite = $CaAl_2Si_2O_8$), clinopyroxene (diopside = $CaMgSi_2O_6$), orthopyroxene

(enstatite = $Mg_2Si_2O_6$), spinel (spinel = $MgAl_2O_4$), and olivine (forsterite = Mg_2SiO_4) were calculated using compositional data and the MELTS software (Ghiorso and Sack, 1995; Asimow and Ghiorso, 1998). MELTS is designed for calculations related specifically to mantle peridotites, but the pyroxene and olivine activities calculated using MELTS are in agreement with activities of these phases determined using AX software (Holland and Powell, 1992; Holland and Powell, 1998).

Calculated endmember activities were used to calculate equilibrium pressure-temperature conditions using THERMOCALC software (Holland and Powell, 1998). Pressures estimated from this analysis range between 550 to 600 MPa. It is likely that the anorthite composition used for barometric purposes is melt related (see discussion on melt refertilization), thus reflecting minimum pressures.

5. DISCUSSION

5.1 Interpretation of microstructures

5.1.1 Overprinting deformations

The bi- and tri- modal grain size distributions exhibited by olivine record a history of overprinting deformations (Nicolas et al., 1971). These grain size distributions reflect changing conditions (stress, strain rate, pressure and/or temperature) during deformation. Compositions of grains from different grain size populations yield different temperature regimes, supporting an interpretation of overprinting deformations.

Undulose extinction, SPO, subgrains, and the development of a LPO indicate dislocation creep accommodated deformation (Goetze and Kohlstedt, 1973; Drury and Urai, 1990; Passchier and Trouw, 2005). Intermediate and fine grain size populations formed as a result of recrystallization-accommodated dislocation creep that overprinted, or partially overprinted, the coarsest grains. The olivine LPO patterns for all grain size populations indicate "pencil glide" defined by slip on the *b* and/or *c* planes in the *a* direction (e.g. (010)[100] and (001)[100] slip systems, respectively).

5.1.2 Phase boundary sliding

Recrystallization-accommodated dislocation creep is suggested by olivine microstructures in both harzburgite and dunite. In harzburgite, straight and aligned phase boundaries between olivine and orthopyroxene grains and microscale olivine and orthopyroxene bands (Figure 5c) suggest phase boundary sliding (PBS) also accommodated deformation (Sundberg and Cooper, 2008). This microstructure,

observed in very coarse-grained harzburgite is similar to aligned phase boundaries observed in both naturally and experimentally deformed fine-grained harzburgite (Newman et al., 1999; Sundberg and Cooper, 2008). Sundberg and Cooper (2008) demonstrate that olivine/orthopyroxene aggregates are weaker than olivine aggregates and suggest that the strength difference results from the ease with which diffusion occurs between the chemically similar minerals as long range diffusion of silica is unnecessary.

Recent experiments have suggested that grain boundary sliding accommodated by dislocation creep (disGBS), as well as diffusion creep, do produce a LPO (Hansen et al., 2011, 2012b), albeit a weaker one than is expected from dislocation creep dominated deformation (Rutter et al., 1994). Furthermore, these mechanisms may weaken a LPO previously formed by dislocation creep. Therefore, an LPO is not definitive evidence that dislocation creep was dominant, and a weak LPO may indicate mechanisms other than dislocation creep were active (Warren and Hirth, 2006; Michibayashi and Oohara, 2013).

The weaker olivine LPO in the Dun Mountain harzburgite samples relative to the dunite samples **(**Figure 7**)**, therefore, suggest that a mechanism other than dislocation creep was active. The straight and aligned grain boundaries between orthopyroxene and olivine in the harzburgite suggests that PBS may have weakened the olivine LPO. Weaker LPO in harzburgites than in neighboring dunites has been recorded in other naturally deformed peridotites (Warren et al., 2008; Webber et al., 2010). Warren et al. (2008) attributed the weaker LPO to dislocation creep-accommodated grain boundary sliding in the harzburgites because of finer olivine grain size in the harzburgites than the

dunites. However, the Dun Mountain harzburgite shows a weaker LPO despite similar grain size and grain size distributions as seen in the dunite, suggesting that a finer grain size is not necessarily the cause of weaker LPO in harzburgite.

5.2 Deformation history

Microstructures and compositions in the Red Hills massif may reflect deformation beginning at the MOR and ending at the forearc as subduction initiated (Stewart et al., in prep.) and trace element profiles of the Dun Mountain samples showing a negative niobium trend are also consistent with a forearc ophiolite (Niu, 2004). Therefore, the overprinting deformations of Dun Mountain likely took place during uplift, within a forearc tectonic setting.

Three generations of olivine grain size indicate 3 episodes of overprinting deformations during recrystallization accommodated dislocation creep. The coarsest grain size population (>4.2 mm) is represented by only olivine so that a temperature estimate is not possible for this coarsest population. Compositions of intermediate grains (1.8 mm) yield 1100-1130 °C while finer grains (0.4 mm) yield 900-950 °C. The decreasing temperature conditions recorded by these samples are consistent with deformation during uplift.

5.2.1 Late melt refertilization

ICP-MS data showing enrichment in both LREEs and HREEs cannot be modeled by any degree of partial melting of fertile or depleted mantle sources and is evidence of melt refertilization (Niu, 2004). Late melt refertilization is supported by the irregular, non-conformable shape of the mesoscale clinopyroxene and plagioclase-bearing dunite pod. Further, microstructures in the plagioclase and clinopyroxene-bearing dunite from this area show irregular and acute grain boundaries indicating melt involvement overprinted deformation microstructures.

5.3 Deformation conditions

Deformation conditions of stress and strain-rate are estimated for 950 and 1100 °C based on geothermometry, using an experimentally derived stress piezometer for olivine (van der Wal et al., 1993) and deformation mechanism maps constructed from experimentally derived flow laws for olivine (e.g., Chopra and Paterson, 1984; Karato et al., 1986; Hirth and Kohlstedt, 1995; Mei and Kohlstedt, 2000; Karato and Jung, 2003).

5.3.1 Stress estimates

Stresses are estimated using an empirically derived stress piezometer in which stress is inversely proportional to the dynamically recrystallized olivine grain size (van der Wal et al., 1993). The chord length averages of the three grain size populations calculated from Spektor's Chord analysis of mean lineal intercept measurements (0.4, 1.8, and 5.0 mm) were used to calculate three stress regimes from the relationship

$$D_g = 0.015^{+0.0004}_{-0.0003}(\sigma) - 1.33 \pm 0.09 \quad (3)$$

where D_g is the grain size (m) from Spektor's Chord analysis and σ is the stress in MPa (Karato et al., 1980; van der Wal et al., 1993). The finest grain size population yields stresses of 15±2 MPa, the intermediate grain size population yields 5±0.5 MPa, while the coarsest population yields 2±0.1MPa.

5.3.2 Deformation mechanism maps

The relationship between strain rate and stress is derived from experiments on polycrystalline olivine and single crystal olivine over a range of P-T and stress conditions. The general flow law is described by the equation

$$\dot{\varepsilon} = A_d \frac{\sigma^n}{d^p} \exp\left[-\frac{E^* + PV^*}{RT}\right] \quad (4)$$

where A_d is a material parameter, σ is the differential stress, n is the stress exponent, d is grain size, p is the grain size exponent, E^* is the activation energy, P is pressure, V^* is the activation volume, R is the gas constant, and T is the absolute temperature (Kohlstedt et al., 1995; Mei and Kohlstedt, 2000; Hirth and Kohlstedt, 2003).

A deformation mechanism map produced using variables defined by Hirth and Kohlstedt (2003) (Table 3) suggests that diffusion creep is dominant at small grain sizes and low stresses, dislocation-accommodated grain boundary sliding (disGBS) is dominant at high stresses and fine grain sizes, and dislocation creep (grain size insensitive) is dominant at coarse grain sizes and higher stresses. Dislocation creep

Table 3

Dry Flow Law Variables

	Hirth and Kohlstedt (2003)			Hansen et al. (2011)		
	Diff	Dis	GBS	Diff	Dis	GBS
A (μm^3/Mpa s	$1.5x10^9$	$1.1x10^5$	6500	$4x10^7$	$1.1x10^5$	$6.3x10^4$
n	1	3.5	3.5	1	3.5	2.9
p	3	0	2	3	0	0.7
E* (kJ/mol)	375	530	400	375	530	445
V* (10^{-6} m^3/mol)	6	18	18	6	18	18

is also promoted by higher P-T conditions, although the flow law is much more sensitive to changes in T than P due to very small V^*. In recent experimental work, Hansen et al. (2011) concluded that disGBS is dominant at lower lithospheric conditions than the Hirth and Kohlstedt (2003) olivine flow law had suggested. Their flow laws have not yet been applied to naturally deformed samples, so I have produced deformation mechanism maps using both flow laws for comparison.

Deformation mechanism maps are created at the two P-T regimes indicated by mineral compositions (1100 °C and 600 MPa, at higher end of the pressure estimate; 950 °C and 550 MPa, the lower end of the pressure estimate) and flow law values from both Hirth and Kohlstedt (2003) and Hansen et al. (2011) (Figure 10). Table 3 lists the flow law variables that were used in the formulation of deformation mechanism maps. Pressure underestimation is a concern in these samples since equilibrium calculations probably reflect low pressures associated with late melt. However, the deformation mechanism maps are fairly pressure-insensitive since the multiplier, V*, is very small (Table 3).

Intermediate and fine olivine grains plotted on maps created using Hirth and Kohlstedt (2003) variables suggest deformation was accommodated by dislocation creep, transitioning towards diffusion creep at finer grain sizes (Figure 10). Calculated strain rates from these flow laws suggest the intermediate and finer grain sizes resulted from deformation at rates of 10^{-13} s^{-1}.

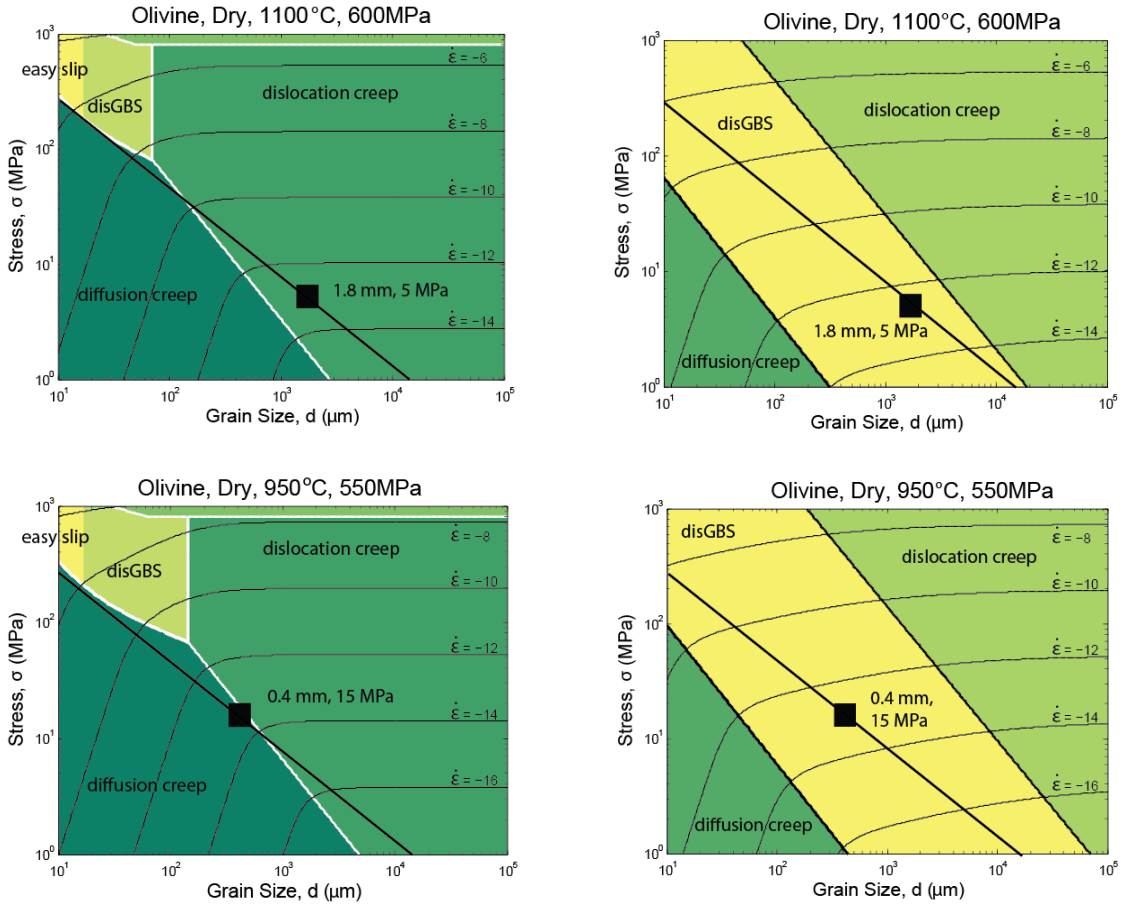

Figure 10: Deformation mechanism maps created using J. Warren's MATLAB program. Maps on the left are created using Hirth and Kohlstedt (2003) flow law variables and maps on the right are created using Hansen et al. (2011) variables (Table 2). Grain size/stress piezometer is superimposed on all maps (van der Wal et al., 1993). Mean grain size from intermediate olivine grains are plotted on the 1100 °C deformation mechanism maps and fine olivine populations are plotted on the 950 °C deformation mechanism maps, consistent with estimated P-T conditions.

Maps created at the same P-T conditions, but with variables reported by Hansen et al. (2011) place greater emphasis on the disGBS regime at lower lithospheric conditions. Intermediate and fine olivine grain sizes plotted on these maps suggest that deformation was accommodated by disGBS for all grain sizes recorded in this study (Figure 10). Strain rates from these flow laws suggest the intermediate and fine grains resulted from deformation between 10^{-12} and 10^{-13} s^{-1}.

5.3.3 Deformations at constant strain rate

The feedback between stress, strain rate, grain size, and P-T conditions during lithospheric deformation is still widely debated. Some workers argue that deformation is controlled by both strain rate and temperature and that stress conditions fluctuate as a result (Dunlap et al., 1997; Behr and Platt, 2011). There is also evidence from both naturally and experimentally deformed rocks that strain localization (i.e. shear zones) requires sufficient grain size reduction to transition to grain-size-sensitive creep (e.g. diffusion creep) and that this will only occur at constant stress (Platt and Behr, 2011; Hansen et al., 2012a).

The Dun Mountain rocks indicate that strain rate remained constant through overprinting deformations over changing P-T conditions and that stress changed in response to these changes in P-T. These samples that deformed in the lithospheric upper mantle are consistent with the conclusions of Dunlap et al. (1997) and Behr and Platt (2011) for lithospheric crust, suggesting that strain rate and temperature controlled stress conditions during deformation, or, that as stress increased, strain rate remained constant.

6. CONCLUSIONS

6.1 Three episodes of overprinting deformations

Analysis of the grain size distribution in porphyroclastic dunite and harzburgite samples from Dun Mountain indicates three separate grain size populations, suggesting overprinting deformation events. The coarsest grains deformed at very low stresses (2 MPa) and were overprinted by subsequent deformations at lower temperature conditions. The intermediate and finer grain sizes record progressively lower temperatures (1100 to 950 °C) and higher stresses (5 to 15 MPa) while overprinting the older mantle fabrics, consistent with changing conditions during uplift. Olivine microstructure in harzburgite and dunite suggest these deformations were accommodated by recrystallization-accommodated dislocation creep in olivine.

6.2 Phase boundary sliding

In harzburgite, olivine and orthopyroxene microstructure (i.e., aligned grain boundaries between olivine and orthopyroxene grains and between microscale olivine and orthopyroxene bands and weaker olivine LPO patterns than observed in dunite samples) suggests PBS accompanied dislocation creep. Similar microstructures have been observed in very fine-grained peridotites in both laboratory and field studies (Newman et al., 1999; Sundberg and Cooper, 2008). The Dun Mountain rocks indicate phase boundary sliding can be important during deformation in coarser-grained harzburgite, as well. Furthermore, similar grain size and grain size distributions in

dunite and harzburgite suggest PBS occurred due to the presence of orthopyroxene, and not due to finer olivine grain sizes.

6.3 Deformations at constant strain rate

Strain rates during overprinting deformations of the Dun Mountain rocks remained constant around 10^{-13} s^{-1} as stresses increased and temperature and pressure decreased. These results, from upper mantle rocks, are consistent with studies of crustal deformation that similarly suggest strain rate is insensitive to changes in deformation conditions (Dunlap et al., 1997; Behr and Platt, 2011).

REFERENCES

Asimow, P. D., and Ghiorso, M. S., 1998, Algorithmic Modifications Extending MELTS to Calculate Subsolidus Phase Relations: American Mineralogist, v. 83, p. 1127-1131.

Barrett, S. D., 2008, Image SXM.

Behr, W. M., and Platt, J. P., 2011, A naturally constrained stress profile through the middle crust in an extensional terrane: Earth and Planetary Science Letters, v. 303, no. 3–4, p. 181-192.

Bohlen, S. R., and Essene, E. J., 1977, Feldspar and oxide thermometry of granulites in the Adirondack Highlands: Contributions to Mineralogy and Petrology, v. 62, no. 2, p. 153-169.

Brace, W. F., and Kohlstedt, D. L., 1980, Limits on lithospheric stress imposed by laboratory experiments: Journal of Geophysical Research: Solid Earth, v. 85, no. B11, p. 6248-6252.

Brey, G. P., and Köhler, T., 1990, Geothermobarometry in Four-phase Lherzolites II. New Thermobarometers, and Practical Assessment of Existing Thermobarometers: Journal of Petrology, v. 31, p. 1353-1378.

Carter, N. L., and Ave'lallemant, H. G., 1970, High temperature flow of dunite and peridotite: Geological Society of America Bulletin, v. 81, no. 8, p. 2181-2202.

Chopra, P. N., and Paterson, M. S., 1984, The role of water in the deformation of dunite: Journal of Geophysical Research: Solid Earth, v. 89, no. B9, p. 7861-7876.

Christensen, N. I., 1984, Structure and origin of the Dun Mountain ultramafic massif, New Zealand: Geological Society of America Bulletin, v. 95, p. 551-558.

DeMets, C., and Dixon, T. H., 1999, New kinematic models for Pacific-North America motion from 3 Ma to present, I: Evidence for steady motion and biases in the NUVEL-1A Model: Geophysical Research Letters, v. 26, no. 13, p. 1921-1924.

Drury, M. R., and Urai, J. L., 1990, Deformation-related recrystallization processes: Tectonophysics, v. 172, p. 235-253.

Dunlap, W. J., Hirth, G., and Teyssier, C., 1997, Thermomechanical evolution of a ductile duplex: Tectonics, v. 16, no. 6, p. 983-1000.

Ghiorso, M. S., and Sack, R. O., 1995, Chemical Mass Transfer in Magmatic Processes. IV. A Revised and Internally Consistent Thermodynamic Model for the Interpolation and Extrapolation of Liquid-Solid Equilibria in Magmatic Systems at Elevated Temperatures and Pressures: Contributions to Mineralogy and Petrology, v. 119, p. 197-212.

Goetze, C., and Kohlstedt, D. L., 1973, Laboratory Study of Dislocation Climb and DIffusion in Olivine: Journal of Geophysical Research, v. 78, no. 26, p. 5961-5971.

Hansen, L. N., Zhao, Y.-H., Zimmerman, M. E., and Kohlstedt, D. L., 2014, Protracted fabric evolution in olivine: Implications for strain measurement and seismic anisotropy: Earth and Planetary Science Letters.

Hansen, L. N., Zimmerman, M. E., Dillman, A. M., and Kohlstedt, D. L., 2012a, Strain localization in olivine aggregates at high temperature: A laboratory comparison

of constant-strain-rate and constant-stress boundary conditions: Earth and Planetary Science Letters, v. 333–334, no. 0, p. 134-145.

Hansen, L. N., Zimmerman, M. E., and Kohlstedt, D. L., 2011, Grain boundary sliding in San Carlos olivine: Flow law parameters and crystallographic-preferred orientation: Journal of Geophysical Research, v. 116, no. B08201.

-, 2012b, The influence of microstructure on deformation of olivine in the grain-boundary sliding regime: Journal of Geophysical Research, v. 117, no. B09201.

Hirth, G., and Kohlstedt, D. L., 1995, Experimental constraints on the dynamics of the partially molten upper mantle: Deformation in the diffusion creep regime: Journal of Geophysical Research: Solid Earth, v. 100, no. B2, p. 1981-2001.

Hirth, G., and Kohlstedt, D. L., 2003, Rheology of the Upper Mantle and the Mantle Wedge: A View from the Experimentalists: Inside the Subduction Factory, v. 138, p. 83-105.

Holland, T., and Powell, R., 1992, Plagioclase feldspars; activity-composition relations based upon Darken's quadratic formalism and Landau theory: American Mineralogist, v. 81, p. 1425-1437.

Holland, T. J. B., and Powell, R., 1998, An internally consistent thermodynamic data set for phases of petrological interest: Journal of Metamorphic Geology, v. 16, p. 309-343.

Karato, S.-I., and Jung, H., 2003, Effects of pressure on high-temperature dislocation creep in olivine: Philosophical Magazine, v. 83, no. 3, p. 401-414.

Karato, S.-I., Paterson, M. S., and FitzGerald, J. D., 1986, Rheology of synthetic olivine aggregates: Influence of grain size and water: Journal of Geophysical Research: Solid Earth, v. 91, no. B8, p. 8151-8176.

Karato, S.-I., Toriumi, M., and Fuji, T., 1980, Dynamic recrystallization of olivine single crystals during high-temperature creep: Geophysical Research Letters, v. 7, no. 9, p. 649-652.

Kohlstedt, D. L., Evans, B., and Mackwell, S. J., 1995, Strength of the lithosphere: Constrains imposed by laboratory experiments: Journal of Geophysical Research, v. 100, no. B9, p. 17587-17602.

Mei, S., and Kohlstedt, D. L., 2000, Influence of water on plastic deformation of olivine aggregates: 2. Dislocation creep regime: Journal of Geophysical Research, v. 159, no. B9, p. 411-427.

Michibayashi, K., and Oohara, T., 2013, Olivine fabric evolution in a hydrated ductile shear zone at the Moho Transition Zone, Oman Ophiolite: Earth and Planetary Science Letters, p. 299-310.

Newman, J., Lamb, W. M., Drury, M. R., and Vissers, R. L. M., 1999, Deformation processes in a peridotite shear zone: reaction-softening by an H2O-deficient, continuous net transfer reaction: Tectonophysics, v. 303, no. 1–4, p. 193-222.

Nicolas, A., Bouchez, J. L., Boudier, F., and Mercier, J. C., 1971, Textures, structures and fabrics due to solid state flow in some European lherzolites: Tectonophysics, v. 12, no. 1, p. 55-86.

Nimis, P., and Grütter, H., 2009, Internally consistent geothermometers for garnet peridotites and pyroxenites: Contributions to Mineralogy and Petrology, v. 159, p. 411-427.

Niu, Y., 2004, Bulk-rock Major and Trace Element Compositions of Abyssal Peridotites: Implications for Mantle Melting, Melt Extraction and Post-melting Processes Beneath Mid-Ocean Ridges: Journal of Petrology, v. 45, no. 12, p. 2423-2458.

Passchier, C. W., and Trouw, R. A., 2005, Microtectonics, Germany, Springer.

Platt, J. P., and Behr, W. M., 2011, Lithospheric shear zones as constant stress experiments: Geology, v. 39, no. 2, p. 127-130.

Regenauer-Lieb, K., Yuen, D. A., and Branlund, J., 2001, The Initiation of Subduction: Criticality by Addition of Water?: Science, v. 294, no. 5542, p. 578-580.

Rutter, E. H., Casey, M., and Burlini, L., 1994, Preferred crystallographic orientation development during the plastic and superplastic flow of calcite rocks: Journal of Structural Geology, v. 16, no. 10, p. 1431-1446.

Stewart et al., in prep.

Sun, S.-s., and McDonough, W. F., 1989, Chemical and isotopic systematics of oceanic basalts: implications for mantle composition and processes: Geological Society, London, Special Publications, v. 42, p. 313-345.

Sundberg, M., and Cooper, R. F., 2008, Crystallographic preferred orientation produced by diffusional creep of harzburgite: Effects of chemical interactions among phases during plastic flow: Journal of Geophysical Research, v. 113, p. B12208.

Taylor, W. R., 1998, An experimental test of some geothermometer and geobarometer formulations for upper mantle peridotites with application to the thermobarometry of fertile lherzolite and garnet webserite: Journal of Mineralogy and Geochemistry, v. 172, p. 381-408.

Toy, V. G., Newman, J., Lamb, W., and Tikoff, B., 2010, The Role of Pyroxenites in Formation of Shear Instabilities in the Mantle: Evidence from an Ultramafic Ultramylonite, Twin Sisters Massif, Washington: Journal of Petrology, v. 51, p. 55-80.

Underwood, E. E., 1970, Quantitative Stereology, Addison-Wesley Publishing Company.

van der Wal, D., Chopra, P., Drury, M., and Gerald, J. F., 1993, Relationships between dynamically recrystallized grain size and deformation conditions in experimentally deformed olivine rocks: Geophysical Research Letters, v. 20, no. 14, p. 1479-1482.

Walcott, R. I., 1965, Structure and Petrology of the Red Hill Complex, Nelson [PhD: Victoria University of Wellington.

Warren, J. M., and Hirth, G., 2006, Grain size sensitive deformation mechanisms in naturally deformed peridotites: Earth and Planetary Science Letters, v. 248, p. 438-450.

Warren, J. M., Hirth, G., and Kelemen, P. B., 2008, Evolution of olivine lattice preferred orientation during simple shear in the mantle: Earth and Planetary Science Letters, v. 272, no. 3–4, p. 501-512.

Webber, C., Newman, J., Holyoke Iii, C. W., Little, T., and Tikoff, B., 2010, Fabric development in cm-scale shear zones in ultramafic rocks, Red Hills, New Zealand: Tectonophysics, v. 489, no. 1–4, p. 55-75.

Webber, C. E., Little, T., Newman, J., and Tikoff, B., 2008, Fabric superposition in the upper mantle peridotite, Red Hills, New Zealand: Journal of Structural Geology, v. 30, p. 1412-1428.

Wells, P., 1977, Pyroxene Thermometry in Simple and Complex Systems: Contributions to Mineralogy and Petrology, v. 62, p. 129-139.